

A quantum picture of light-suppressed photosynthetic charge transfer: Photo-blockade

Guang Yang^{a)} and Gen Tatara

RIKEN Cluster for Pioneering Research, Wako, Saitama 351-0198, Japan

(Dated: 22 March 2024)

We propose a dynamic mechanism for the reversible regulation of photochemistry in plants under varying light environments. We employ a three-level quantum model to take into account the correlations between charge donors and charge acceptors immediately before photoexcitation, and show that under steady and coherent driving of light, the efficiency of charge transfer is inversely proportional to the intensity of incident light, which can be suppressed so severely that it becomes a limiting factor on photosynthetic electron transport. These results are analyzed to gain insight in the light responses of photosynthetic parameters. We discuss the implications of thermal fluctuation in the light source used in photochemical experiments, and argue that in high light conditions, the quantum yields measured with an incandescent lamp may be higher than those measured with a laser, a manifestation of thermal fluctuation in lamp illumination. Our new picture renders a consistent interpretation of a wide range of experiments, including plastocyanin-dependent electron transport in photosystem I, biphasic redox kinetics of P700 and wavelength-dependent quantum yields, and provides a donor-side scheme for the onset of irreversible damage to photosystem II.

I. INTRODUCTION

A central topic in plant physiology has been to understand the dynamic regulation and acclimation of the photosynthetic machinery in changing light environments. Plants in natural habitats, for instance, are subject to fluctuations of ambient light from cloud and canopy covering. To deal with fluctuating light, a fast and efficient control of the yields of photosynthetic reactions is necessary to ensure a regulated electron flow through the functional units and to channel away the excess excitation energy delivered from light-harvesting antennas, thus avoiding congestion and overheating of the whole machinery. Past experiments have indeed demonstrated that photosystem I (PSI) and photosystem II (PSII), two functional units where the primary photochemistry takes place, are capable of exceptionally flexible adjustments of photochemical efficiencies in response to varying ambient light.¹ At increasing light intensities, PSI and PSII tune down the chloroplast electron transport in a remarkably concerted fashion and dissipate most of the excess energy as heat.

Traditionally, light-induced down-regulation of photochemistry has been attributed to feedback mechanisms caused by an elevated proton gradient (ΔpH) across the thylakoid membrane.² In higher light conditions, the metabolic consumption of ATP in carbon fixation declines and proton efflux through the ATP synthase slows down, resulting in an increasingly acidic thylakoid lumen. Acidification of the lumen then triggers non-photochemical quenching (NPQ)³ of excessively absorbed light energy and imposes a constriction on the linear electron flow (LEF) at the cytochrome (Cyt) *b6f* complex located between PSI and PSII, a commonly recognized safety valve in photosynthetic electron transport chain. Accordingly, the yield of PSI and subsequently that of PSII are diminished. In addition to LEF, proton pumping associated with various cyclic electron flow (CEF) pathways around PSI is believed

to play a supplemental role in generating ΔpH .⁴⁻⁷ Fig. 1(a) shows the pathways of LEF and CEF, along with the redox potentials of the intermediate steps.

The ΔpH -dependent scheme of photosynthetic control, despite its general acceptance, is not without questions. Experiments showed that NPQ saturated at a notably higher light intensity than LEF, indicating the insufficient role of LEF in inducing regulatory feedback in high light and the existence of other variables. This was referred to as the evidence of a growing portion of CEF in PSI turnover contributing additional ΔpH .⁸ A CEF-based model of photosynthesis regulation, nevertheless, is somewhat paradoxical, as it suggests that an accelerated portion of electron transport via Cyt *b6f*, in the form of CEF, simultaneously slows down the overall electron transport at the same location.⁹ Even more importantly, the ΔpH -dependent scheme does not explain the observation that the yields of PSI and PSII are both much more sensitive to light environments than NPQ, the modulation of which occurs not only in a fast, dynamic and interconnected fashion,¹⁰ but starts in low light, well preceding the activation of NPQ.¹¹ Indeed, a series of recent experiments confirmed that the elevation of ΔpH was negligible in low light,¹² and cast doubt on the causal relationship between NPQ and electron transport in PSI.⁹⁻¹¹ This calls for a reconsideration of the mechanism regulating photosynthetic reactions in varying light conditions.

In this paper, we propose a quantum mechanical picture of the regulation of electron transport through photosystems, dubbed photo-blockade, based on suppressed charge transfer on the donor sides of PSI and PSII under coherent driving of light. Quantum coherence has been shown to play an important role in the highly efficient transfer of excitation energy from light-harvesting antennas to photosynthetic reaction centers (see Ref. 13 for a review of theoretical modeling of collective exciton states and coherent energy transport). Here we demonstrate its significance in interpreting charge transfer data. Specifically, we adopt a simple model of three quantum levels to account for the essential steps in electron transport before and during photoexcitation, and show that the interplay of quantum correlations between these levels and light-matter

^{a)}Electronic mail: guang.yang@riken.jp

interaction can lead to a suppression of the forward transfer rate of electrons, the extent of which is proportional to the intensity of light. This finding is a rather general one, and offers an alternative explanation of the dynamic and coordinated responses of PSI and PSII to light changes, in which the oxidation of plastocyanin (PC), rather than that of plastoquinol (PQH_2), is the rate-limiting step on LEF. Down-regulation of photochemical efficiencies is thus understood to be a direct action of light, rather than one depending on feedback mechanisms to light-induced fluctuations in the electron transport. Using this picture, we discuss the characteristics of the light response curves of photosynthetic parameters.^{14–17} Interestingly, our model allows for a new donor-side interpretation of the PSI parameter Y(NA), previously believed to reflect the acceptor-side limitation on LEF. We argue that photo-blockade serves as a mechanism of photoprotection. In dim light, its effect is less significant and the oxidation of reaction center chlorophylls, P700 in PSI and P680 in PSII, is driven by incoherent photoexcitation of electrons from the ground-state electron transport molecules. As incident light gets stronger, both PSI and PSII undergo a transition from incoherent to coherent photoexcitation. Eventually, LEF is entirely governed by photo-blockade, which determines the steady-state Y(NA) and the reduction rates of oxidized P700 and P680 ($P700^+$ and $P680^+$), thus preventing the passage of excess charge excitations. Under extreme environmental stresses, quantum coherence underlying photo-blockade may be destroyed. Without its protection, incoherently excited electrons flood the acceptor side of PSI, signaled by an anomalous rise in Y(NA),^{7,11,18} leading to unregulated charge recombination and a malfunctioning PSI.⁴

Our model may also shed light on the observed biphasic reduction kinetics of $P700^+$ after saturating illumination.^{19,20} Photo-blockade suppresses charge transfer from PC to $P700^+$ and creates a local charge imbalance. Upon cessation of the flash, local equilibration between PC and $P700^+$ occurs first on a shorter time scale, followed by global reduction of the entire electron transport chain by LEF on a longer time scale. This kinetics is indeed biphasic. In principle, establishment of the local charge imbalance is immediate after illumination is turned on. In reality, however, heterogeneity in the distribution of charge carriers exists across different luminal compartments, and it may take a finite time for the PC pool to reach steady-state redox status at a given light intensity. A corollary of this is that a very short flash is not capable of driving and stabilizing a local charge imbalance between PC and $P700$, and thus the $P700$ redox kinetics exhibits less biphasic features.²¹ We postulate moreover that in steady state, an over-reduced PC pool may induce a backreaction on the plastoquinone (PQ) pool and the acceptor side of PSII, causing a drop in the quantum yield of PSII, which may find indications in the absorbance data of Cyt *b6f*.

In a similar vein, the photo-blockade picture may prove helpful in understanding irreversible photodamage to PSII, previously associated with over-reduced quinone acceptors facilitating production of harmful reactive oxygen species,²² but now increasingly accepted to result from blocked charge transfer from the oxygen-evolving manganese cluster to $P680^+$ mediated by tyrosines Z and D (TyrZ and TyrD).^{23–28}

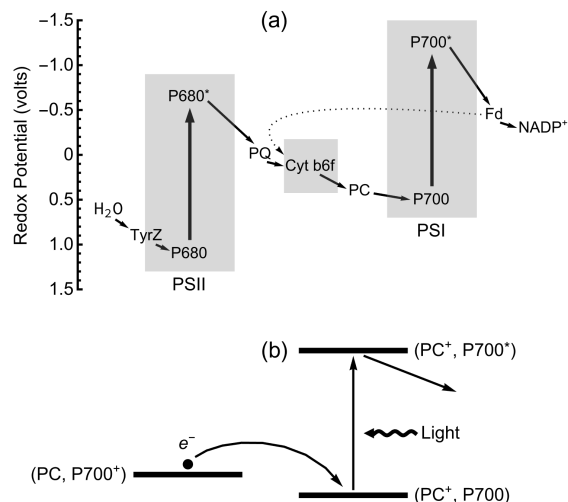


FIG. 1. (a) Pathways of linear electron flow (solid arrows) through photosystems I and II, via cytochrome *b6f* complex and assisted by two types of charge carriers plastoquinone and plastocyanin, and cyclic electron flow (dotted arrow) around photosystem I, from ferredoxin back to cytochrome *b6f* complex. (b) A three-level system as a minimal model to study the effect of quantum coherence on photoexcitation, taking photosystem I as an illustrative example, in which an electron may occupy a plastocyanin state, the P700 ground state, or the P700 excited state, corresponding to configuration $(PC, P700^+)$, $(PC^+, P700)$, or $(PC^+, P700^*)$, respectively, and will finally relax to outside the system (*i.e.*, to next step in the electron transport chain).

A new hypothesis is that the blocked charge transfer is due to light-induced inactivation of the manganese cluster, which then leads to aggregation of highly oxidizing and damaging $P680^+$ on the donor side.^{25,26} Photo-blockade, a direct effect of light, provides a different account of the abnormally long-lived $P680^+$,^{27,28} and unifies the primary causes of irreversible photodamage and reversible light responses in the spirit of the Principle of Simplicity – a simple general principle is often buried underneath a seemingly complex set of processes.

The workings of photo-blockade rely on the availability of pathways to dissipate excess excitation energy. We suggest that photo-blockade acts as a zeroth-order regulator of photochemistry, whereas ΔpH -dependent mechanisms play the vital roles of an energy dissipator, an LEF fluctuation sensor and an overall redox homeostasis stabilizer, ensuring balanced charge and energy transfer in chloroplasts, in conjunction with other feedback processes that are essential in low light in the absence of a large ΔpH to activate NPQ, including charge recombination,^{4,11} CEF around PSI,^{4–7} light-induced size changes of granal thylakoid lumen,²⁰ and phosphorylation-enhanced energy exchange between PSI and PSII.²⁹

This paper is organized as follows. In Sec. II, we model and study photo-blockade effect in an isolated system and in an open system interacting with an environment. In Sec. III, we use the results from Sec. II to interpret experimental data and discuss further implications. We propose an experiment to test our model and conclude in Sec. IV.

II. MODEL

We consider the electronic dynamics on the donor sides of PSI and PSII, where electrons are transferred from the immediate donors, PC and TyrZ (as well as TyrD) respectively, to P700 and P680, and then are excited upon absorption of photons to create excited states P700* and P680* which further pass on the electrons to form primary charge separations. The electronic system of interest at PSI is a three-level one, illustrated in Fig. 1(b), with an electron possibly occupying a PC state, denoted by a quantum state $|L\rangle$ and corresponding to the configuration (PC, P700⁺), or occupying the ground state of P700, denoted by $|R\rangle$ and corresponding to the configuration (PC⁺, P700), or occupying the excited state of P700, denoted by $|R^*\rangle$ and corresponding to the configuration (PC⁺, P700*). Here PC⁺ stands for oxidized PC. Similar definitions are implied for the discussion of PSII.

The system under consideration is not in thermal equilibrium but is one coherently driven by light. To model the dynamic effects in such a driven system, we single out the photon mode most resonant with excitation of electrons and adopt a full quantum mechanical description of its interactions by the Jaynes–Cummings model.³⁰ A similar idea is often employed in the lab, where a laser or a filtered monochromatic light is used to measure the light responses of photosynthetic parameters. The Hamiltonian is

$$H = \begin{pmatrix} \Delta_1 & \Gamma & 0 \\ \Gamma & 0 & ga^\dagger \\ 0 & ga & \Delta_2 \end{pmatrix} + \omega a^\dagger a, \quad (1)$$

where a^\dagger is the photon creation operator, ω is the photon energy, and g is the electron-photon coupling strength. Δ_1 and Δ_2 are the energy differences between $|L\rangle$ and $|R\rangle$ and between $|R\rangle$ and $|R^*\rangle$, respectively. Γ is the experimentally tunable transition amplitude between $|L\rangle$ and $|R\rangle$ in the redox reaction.³¹ In PSI photochemistry, for instance, application of PC inhibitors effectively reduces the statistical average of Γ .³² We set $\hbar = 1$ throughout the paper.

In what follows we study this Hamiltonian, first in an isolated system and then in an open system subject to environment-induced relaxation. In an isolated system, the total population of the electron is unity and the local charge is conserved. In an open system, the electron eventually vanishes from the system via photoexcitation and subsequent decay into environment. Later when we use the open system model to describe electron transport in PSI and PSII, we assume that there is a steady and uniform supply of electrons into $|L\rangle$ such that the local charge is still more or less conserved. Moreover, owing to the existence of a large redox potential gradient upstream, we assume negligible back-tunneling of electrons from $|L\rangle$. Thus, the flow of electrons is largely one-way and we focus on studying time evolution of the system with an electron initially in $|L\rangle$. Deviations of realistic transport from the description of a single electron model with a conserved local charge will be discussed in Sec. III.

A. Isolated system: suppressed quantum tunneling

Consider an isolated system described by the Hamiltonian in Eq. (1). We are interested in the population dynamics of an electron initially occupying $|L\rangle$. Three different initial states of photons are included in the analysis, a Fock state, a coherent state, and a thermal state. A Fock state enjoys the mathematical simplicity of a fixed photon number and serves as a comparative example. A coherent state is an idealized quantum description of a laser. A thermal state contains a considerable amount of thermal fluctuation and is representative of an optically filtered incandescent lamp sometimes used in photochemical experiments. We assume that the system is initially separable,³³ *i.e.*, at $t = 0$ the system is described by a product of the density matrices of the electron and the photons, $\rho_{\text{tot}}(0) = \rho(0) \otimes \rho_{\text{ph}}(0)$, where the electron density matrix $\rho(0) = |L\rangle\langle L|$. At time t , the total density matrix $\rho_{\text{tot}}(t) = e^{-iHt} \rho_{\text{tot}}(0) e^{iHt}$.

1. Fock state

We first study a Fock state of n photons at $t = 0$, described by $\rho_{\text{ph}}(0) = |n\rangle\langle n|$. We define the shorthand notation $|L, n\rangle = |L\rangle \otimes |n\rangle$. The Hamiltonian can be cast in a block-diagonal form in the Hilbert space spanned by $|L, n\rangle$, $|R, n\rangle$, $|R^*, n-1\rangle$,

$$H_n = \begin{pmatrix} \Delta_1 & \Gamma & 0 \\ \Gamma & 0 & g_n \\ 0 & g_n & \Delta \end{pmatrix} + n\omega \mathbf{1}_{3 \times 3}, \quad (2)$$

where $g_n = g\sqrt{n}$, and $\Delta = \Delta_2 - \omega$ is the energy mismatch between incident photons and the electronic transition, sometimes referred to as the detuning. The constant term $n\omega \mathbf{1}_{3 \times 3}$ contributes a phase in the wave functions but disappears in density matrices. We neglect this term henceforth, which amounts to working in the interaction picture.

Let $|\Psi_n(t)\rangle = e^{-iH_n t} |\Psi_n(0)\rangle$ be the total wave function at time t , where $|\Psi_n(0)\rangle = |L, n\rangle$. Then $\rho_{\text{tot}}(t) = |\Psi_n(t)\rangle\langle\Psi_n(t)|$. The reduced density matrix of the electron is obtained by tracing out the photon field, $\rho(t) = \text{Tr}_{\text{ph}} \rho_{\text{tot}}(t)$, whose diagonal elements $\rho^L(t)$, $\rho^R(t)$, $\rho^{R^*}(t)$ give the probabilities of finding the electron in $|L\rangle$, $|R\rangle$, $|R^*\rangle$, respectively, at a given time. In Fig. 2, we show numerically calculated time-dependent population in $|L\rangle$ for different parameter settings. We find that in general, quantum tunneling of the electron from the initial state $|L\rangle$ is suppressed at large photon numbers. This holds true regardless of the choices of the redox potential difference Δ_1 and the detuning Δ .

We are thus motivated to invoke an analytical approach to a better understanding of this localization effect. For simplicity, we assume degenerate $|L\rangle$ and $|R\rangle$, and solve the Schrödinger equation to obtain a solution of the form (see Appendix A),

$$|\Psi_n(t)\rangle = c_{1,n}(t)|L, n\rangle + c_{2,n}(t)|R, n\rangle + c_{3,n}(t)|R^*, n-1\rangle, \quad (3)$$

with which we find the analytical expressions of density matrices. A further simplification of the results is rendered with

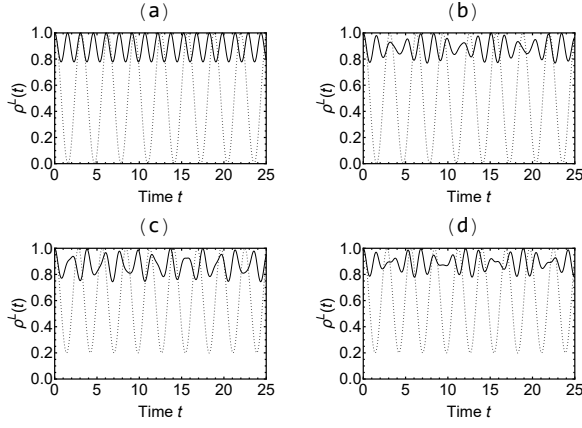


FIG. 2. Time-dependent population in $|L\rangle$ of an electron interacting with a Fock state of $n = 16$ (solid curves) and $n = 0$ (dotted curves) photons in an isolated system. The parameters are $\Delta_1 = 0$ and $\Delta = 0$ in (a), $\Delta_1 = 0$ and $\Delta = 1$ in (b), $\Delta_1 = 1$ and $\Delta = 0$ in (c), and $\Delta_1 = 1$ and $\Delta = 1$ in (d). In all the plots $g = \Gamma = 1$.

the assumption of a zero detuning, *i.e.*, the incident photons are resonant with the electronic transition from $|R\rangle$ to $|R^*\rangle$. The eigenvectors of H_n are then found to be

$$\begin{aligned} |0, n\rangle &= \cos \theta_n |L, n\rangle - \sin \theta_n |R^*, n-1\rangle, \\ |+, n\rangle &= \frac{\sin \theta_n}{\sqrt{2}} |L, n\rangle + \frac{1}{\sqrt{2}} |R, n\rangle + \frac{\cos \theta_n}{\sqrt{2}} |R^*, n-1\rangle, \\ |-, n\rangle &= \frac{\sin \theta_n}{\sqrt{2}} |L, n\rangle - \frac{1}{\sqrt{2}} |R, n\rangle + \frac{\cos \theta_n}{\sqrt{2}} |R^*, n-1\rangle, \end{aligned} \quad (4)$$

with eigenvalues $0, \lambda_n, -\lambda_n$, respectively, where $\tan \theta_n = \Gamma/g_n$ and $\lambda_n = \sqrt{\Gamma^2 + g_n^2}$. The eigenvector $|0, n\rangle$, having a vanishing $|R\rangle$ component, is known as a “dark state” in optics.³⁴ (Note that this is different from symmetry-forbidden states in dipole transitions,³⁵ *e.g.*, a carotenoid “dark state”.)

We rewrite the initial total wave function in terms of the eigenvectors,

$$|\Psi_n(0)\rangle = \cos \theta_n |0, n\rangle + \frac{\sin \theta_n}{\sqrt{2}} (|+, n\rangle + |-, n\rangle), \quad (5)$$

to find its time evolution. At time t , the total wave function has the form of Eq. (3), with

$$\begin{aligned} c_{1,n}(t) &= \cos^2 \theta_n + \sin^2 \theta_n \cos \lambda_n t, \\ c_{2,n}(t) &= -i \sin \theta_n \sin \lambda_n t, \\ c_{3,n}(t) &= \sin \theta_n \cos \theta_n (\cos \lambda_n t - 1), \end{aligned} \quad (6)$$

and the diagonal matrix elements $\rho^L(t) = |c_{1,n}(t)|^2$, $\rho^R(t) = |c_{2,n}(t)|^2$, and $\rho^{R^*}(t) = |c_{3,n}(t)|^2$. In Eq. (6), the only time dependence is through $\cos \lambda_n t$ (or $\sin \lambda_n t$). Thus, we may obtain time-averaged populations over a single oscillatory period $[0, 2\pi/\lambda_n]$, by setting $\cos \lambda_n t = 0$ and $\cos^2 \lambda_n t = 1/2$. Let

$P_L = \overline{\rho^L(t)}$, $P_R = \overline{\rho^R(t)}$, and $P_{R^*} = \overline{\rho^{R^*}(t)}$. We find

$$\begin{aligned} P_L &= \cos^4 \theta_n + \frac{1}{2} \sin^4 \theta_n, \\ P_R &= \frac{1}{2} \sin^2 \theta_n, \\ P_{R^*} &= \frac{3}{2} \sin^2 \theta_n \cos^2 \theta_n. \end{aligned} \quad (7)$$

It is easy to verify that $P_L + P_R + P_{R^*} = 1$, *i.e.*, the total population is conserved.

We are interested in the “leaked population” out of $|L\rangle$, defined as $\delta P_L = 1 - P_L$, as a measure of the suppression of quantum tunneling. Using $\sin^2 \theta_n = \Gamma^2/(\Gamma^2 + g_n^2)$, we find $\delta P_L = \delta P_{L,1} - \delta P_{L,2}$, where

$$\begin{aligned} \delta P_{L,1} &= \frac{2}{1 + \varepsilon n}, \\ \delta P_{L,2} &= \frac{3/2}{(1 + \varepsilon n)^2}, \end{aligned} \quad (8)$$

with $\varepsilon = g^2/\Gamma^2$. As a quick check, at $n = 0$ we have $\delta P_L = 1/2$, and thus there is 50% probability that the electron is in $|L\rangle$. This is certainly true, because when there is no photon in the system, $|R^*\rangle$ decouples from $|L\rangle$ and $|R\rangle$, and the electron oscillates between $|L\rangle$ and $|R\rangle$ with equal probabilities. On the other hand, as $n \rightarrow \infty$, $\delta P_L \rightarrow 0$, *i.e.*, the electron is permanently locked in $|L\rangle$. This is again expected, because in this case $\sin \theta_n \rightarrow 0$, and the initial state $|\Psi_n(0)\rangle = |L, n\rangle$ approaches the dark state $|0, n\rangle$ in Eq. (4). Thus, the electron will remain in the initial state indefinitely. We emphasize that the occurrence of suppression of quantum tunneling does not depend on the convenient mathematical conventions chosen here, as shown in Fig. 2, or the realization of a true dark state which is very unlikely in natural environments.

The new parameter ε is related to the intensity of incident light. To see this, notice that g is in fact the polarization energy due to coupling of the atomic dipole with the electric field carried by one incident photon,³⁴

$$g = -\vec{\xi} \cdot \vec{d} \sqrt{\frac{\omega}{2\mu_0 V}}, \quad (9)$$

where $\vec{\xi}$ is the polarization vector of the photon, $\vec{d} = \langle R | \hat{d} | R^* \rangle$ is the dipolar interaction matrix element assumed to be real without loss of generality, μ_0 is vacuum permittivity, and V is the size of the system. The electric field strength is simply the amplitude of canonically quantized field in the Coulomb gauge,

$$\vec{\mathcal{E}} = \vec{\xi} \sqrt{\frac{\omega}{2\mu_0 V}} (a + a^\dagger), \quad (10)$$

in the long-wavelength limit assumed for a bound-state electron in the Jaynes–Cummings model. At the same time, Γ defined in Eq. (1) also has the dimension of energy, $\Gamma = \langle L | \hat{A} | R \rangle$, where \hat{A} is the tunneling operator between $|L\rangle$ and $|R\rangle$. Thus,

$$\varepsilon = \frac{|\langle R | \vec{\xi} \cdot \hat{d} | R^* \rangle|^2}{|\langle L | \hat{A} | R \rangle|^2} \mathcal{E}^2 \quad (11)$$

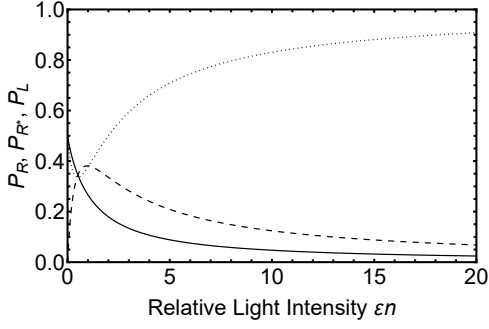


FIG. 3. Time-averaged steady-state populations in $|R\rangle$ (solid curve), $|R^*\rangle$ (dashed curve) and $|L\rangle$ (dotted curve) of an electron interacting with a Fock state of photons in an isolated system, as functions of the relative light intensity.

is a dimensionless quantity proportional to the squared electric field strength of a single photon and inversely proportional to the system size. In the classical picture, $\mu_0 \mathcal{E}^2$ is the energy density of an electromagnetic wave. Thus, heuristically, ε may be interpreted as proportional to the energy density of the electromagnetic radiation created by a single photon, and εn is proportional to the total energy density of all incident photons, *i.e.*, the macroscopic intensity of light. In an optical cavity of a finite size, photon number is a meaningful quantity. In free space such as a natural environment, however, $\varepsilon n \propto n/V$ is physically more significant. We define the macroscopic limit

$$n \rightarrow \infty, \quad \varepsilon \rightarrow 0, \quad \varepsilon n \rightarrow \text{constant}. \quad (12)$$

Eq. (8) thus describes the suppression of quantum tunneling as a function of the macroscopic light intensity. In high light conditions with $\varepsilon n \gg 1$, the contribution of $\delta P_{L,2}$ is negligible, and $\delta P_L \rightarrow \delta P_{L,1}$. In fact, using $\sin^2 \theta_n = 1/(1 + \varepsilon n)$, we see that the steady-state populations in Eq. (7) are all macroscopic quantities, which we plot in Fig. 3.

By Eq. (11), εn is determined not only by the absolute light intensity, but relative to the bare parameter Γ . We will refer to it as the relative light intensity.

2. Coherent state

Next, we study quantum tunneling of the electron assuming that the photons are initially in a coherent state described by $\rho_{\text{ph}}(0) = |\alpha\rangle\langle\alpha|$, where

$$|\alpha\rangle = e^{-\frac{\alpha^2}{2}} \sum_{n=0}^{\infty} \frac{\alpha^n}{\sqrt{n!}} |n\rangle \quad (13)$$

is the coherent state wave function in the photon-number basis. We have assumed without loss of generality that α is real. The probability of finding n photons in $|\alpha\rangle$ follows a Poisson distribution

$$p_{\alpha,n} = e^{-m_\alpha} \frac{(m_\alpha)^n}{n!}, \quad (14)$$

where $m_\alpha = \alpha^2$ is the mean photon number.

As in the treatment of a Fock state, we assume $\Delta_1 = \Delta = 0$ and rewrite the initial total wave function $|\Psi(0)\rangle = |L, \alpha\rangle$ in terms of the eigenvectors in Eq. (4) to find its time evolution. The total wave function at time t is

$$|\Psi(t)\rangle = e^{-\frac{\alpha^2}{2}} \sum_{n=0}^{\infty} \frac{\alpha^n}{\sqrt{n!}} |\Psi_n(t)\rangle, \quad (15)$$

where $|\Psi_n(t)\rangle$ is defined in Eq. (3) and the coefficients are given in Eq. (6). We then have $\rho(t) = \text{Tr}_{\text{ph}} |\Psi(t)\rangle\langle\Psi(t)|$. Upon performing time average on $\rho^L(t)$, $\rho^R(t)$, and $\rho^{R^*}(t)$, we find the leaked population out of $|L\rangle$, $\delta P_L = \delta P_{L,1} - \delta P_{L,2}$, with

$$\begin{aligned} \delta P_{L,1} &= \sum_{n=0}^{\infty} p_{\alpha,n} \frac{2}{1 + \varepsilon n}, \\ \delta P_{L,2} &= \sum_{n=0}^{\infty} p_{\alpha,n} \frac{3/2}{(1 + \varepsilon n)^2}. \end{aligned} \quad (16)$$

These results differ from those in Eq. (8) for a Fock state by a summation over photon number, weighted by the Poisson distribution $p_{\alpha,n}$ defining the coherent state. In Appendix B, we show the compact expressions of $\delta P_{L,1}$ and $\delta P_{L,2}$ as functions of ε and m_α . Numerical calculation (not shown) confirms that $\delta P_{L,2}$ becomes vanishingly small at large photon numbers $m_\alpha \gg 1$ for fixed ε , or in high light conditions $\varepsilon m_\alpha \gg 1$ in the macroscopic limit $m_\alpha \rightarrow \infty$ and $\varepsilon \rightarrow 0$.

When $m_\alpha \gg 1$ and $\varepsilon \ll 1$, the leading-order terms in the asymptotic expansion of $\delta P_{L,1}$ are (see Appendix B)

$$\delta P_{L,1} = \frac{2}{1 + \varepsilon m_\alpha} \left(1 + \frac{\varepsilon^2 m_\alpha}{(1 + \varepsilon m_\alpha)^2} + \dots \right). \quad (17)$$

Finite-size effects at a given relative light intensity εm_α are encoded in the leading-power terms in $\varepsilon \propto V^{-1}$, which may be explored in a cavity experiment. Moreover, taking the macroscopic limit, we find

$$\delta P_{L,1} = \frac{2}{1 + \varepsilon m_\alpha}, \quad (18)$$

which agrees in the form with the result for a Fock state. This is hardly surprising, however, as the relative uncertainty in photon number of a coherent state vanishes macroscopically, so that the statistical quantities are well approximated by their mean values.

3. Thermal state

Last, we consider a thermal state of photons interacting with the electron. A thermal state is a mixed quantum state, described by $\rho_{\text{ph}}(0) = \sum_{n=0}^{\infty} p_{\beta,n} |n\rangle\langle n|$, where

$$p_{\beta,n} = \frac{(m_\beta)^n}{(m_\beta + 1)^{n+1}}, \quad (19)$$

with $m_\beta = 1/(e^{\beta\omega} - 1)$ the mean photon number and $\beta = 1/k_B T$ the inverse temperature. Unlike a coherent state, a thermal state hosts a large amount of thermal fluctuation, and the

relative uncertainty in photon number does not vanish in the macroscopic limit. The initial and time-dependent total density matrices are $\rho_{\text{tot}}(0) = \sum_{n=0}^{\infty} p_{\beta,n} |L, n\rangle \langle L, n|$ and $\rho_{\text{tot}}(t) = \sum_{n=0}^{\infty} p_{\beta,n} |\Psi_n(t)\rangle \langle \Psi_n(t)|$, respectively, where $|\Psi_n(t)\rangle$ is given in Eqs. (3)(6).

Following the previous procedures, we perform time average on the density matrix elements and obtain the leaked population $\delta P_L = \delta P_{L;1} - \delta P_{L;2}$, with

$$\begin{aligned} \delta P_{L;1} &= \sum_{n=0}^{\infty} p_{\beta,n} \frac{2}{1 + \varepsilon n}, \\ \delta P_{L;2} &= \sum_{n=0}^{\infty} p_{\beta,n} \frac{3/2}{(1 + \varepsilon n)^2}. \end{aligned} \quad (20)$$

The expressions of $\delta P_{L;1}$ and $\delta P_{L;2}$ as functions of ε and m_{β} are given in Appendix B. At large photon numbers, $\delta P_{L;2}$ is negligible.

We study $\delta P_{L;1}$ in the macroscopic limit $m_{\beta} \rightarrow \infty$ and $\varepsilon \rightarrow 0$, demanding that $\varepsilon m_{\beta} > 1$ to avoid obtaining unphysical probabilities that are either negative or greater than one. When $\varepsilon m_{\beta} \ll 1$, one must include both $\delta P_{L;1}$ and $\delta P_{L;2}$ for a correct estimation of the degree of suppressed quantum tunneling. The lowest-order terms in the expansion of $\delta P_{L;1}$ are (see Appendix B)

$$\delta P_{L;1} = \frac{2}{\varepsilon m_{\beta}} \left(\ln \varepsilon m_{\beta} - \gamma_0 + \dots \right), \quad (21)$$

where γ_0 is Euler's constant.

A major difference between a thermal state and a coherent state (or a Fock state) is that the suppression of quantum tunneling is weakened in the former case due to the presence of thermal fluctuation introduced by photons partly destroying the quantum coherence underlying localization of the electron, reflected by an extra logarithm factor in the leaked population, Eq. (21). This weakening effect originates from an incoherent superposition of different photon-number components in a thermal state and is *not* damping in nature. In very high light, $\delta P_{L;1} \rightarrow 0$ because $1/x$ decays faster than $\ln x$ grows, and the electron will be permanently localized in $|L\rangle$.

In Fig. 4, we compare exact results of δP_L for a Fock state, a coherent state and a thermal state, given in Eqs. (8)(16)(20), as functions of (mean) photon numbers $\langle n \rangle = n$, m_{α} and m_{β} , respectively. At large photon numbers, δP_L for a coherent state and for a Fock state become hardly discernible, whereas that for a thermal state diminishes at a much slower rate. In addition, we notice the existence of maxima at some finite photon numbers before δP_L decays asymptotically. Mathematically, $\delta P_{L;2}$ are of comparable orders of magnitudes as (but still smaller than) $\delta P_{L;1}$ near these maxima. Physically, the electron is least localized in $|L\rangle$. Thus, upon increasing the intensity of light from zero, an electron in $|L\rangle$ is first leaked out to $|R\rangle$ and $|R^*\rangle$, and later trapped back in $|L\rangle$. A further numerical analysis (not shown) confirms the generality of this finding and that the locations of maxima move towards zero photons at larger ε settings. Variation of ε at a given photon number exhibits a similar behavior of δP_L . The maxima move closer to $\varepsilon = 0$ when a larger photon number is chosen. This

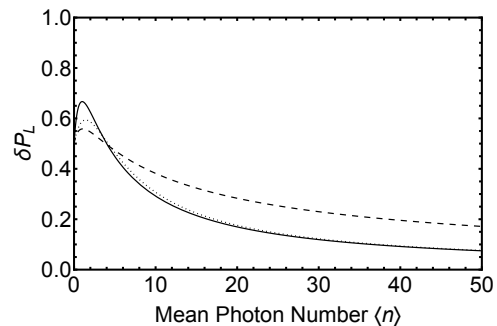


FIG. 4. Exact results of leaked population outside $|L\rangle$ of an electron in an isolated system interacting with a Fock state (solid curve), a thermal state (dashed curve) and a coherent state (dotted curve) of photons, as functions of (mean) photon numbers $\langle n \rangle = n$, m_{β} and m_{α} , respectively. The parameters are $\Delta_1 = \Delta = 0$ and $\varepsilon = 0.5$.

is not surprising since ε and photon number enter the expressions of populations as a symmetric product. To first order, they should affect the populations in a similar fashion.

4. Linear entropy

To see the direct effect of thermal fluctuation in photons on the electronic state, we numerically calculate linear entropy

$$S(t) = 1 - \text{Tr} \rho^2(t), \quad (22)$$

which measures the degree of mixture in a quantum state, and vanishes in a pure state, *e.g.*, for a Fock state of photons. To this end, we must truncate the infinite summation in the photon density matrix. For a thermal state, for instance, we replace $\rho_{\text{ph}}(0) = \sum_{n=0}^{\infty} p_{\beta,n} |n\rangle \langle n|$ with

$$\begin{aligned} \rho_{\text{ph}}^a(0) &= \sum_{n=0}^N p_{\beta,n} |n\rangle \langle n|, \\ \rho_{\text{ph}}^b(0) &= \sum_{n=0}^{N-1} p_{\beta,n} |n\rangle \langle n| + \left(1 - \sum_{n=0}^{N-1} p_{\beta,n} \right) |N\rangle \langle N|, \end{aligned} \quad (23)$$

and determine a choice of N that yields negligible differences in the numerical results obtained using $\rho_{\text{ph}}^a(0)$ and $\rho_{\text{ph}}^b(0)$. We then use either method of truncation for the calculation.

In general, we find that a thermal state of photons delivers more mixture to the electron than a coherent state of photons, indicated by a larger linear entropy. Moreover, the linear entropy is smaller for fewer incident photons, where the electron is less contaminated, reaches a maximum at an intermediate photon number, and diminishes towards zero at larger photon numbers where the electronic state becomes purer again as photons drive it towards an eigenstate of the Hamiltonian. In a thermal state, but not in a coherent state, we find an increasingly exact anti-correlation between the linear entropy and the population in $|L\rangle$ when the photon number is large enough, an example shown in Fig. 5(a), independent of the choice of parameters such as the detuning. In a coherent state, we observe collapses and revivals of Rabi oscillation of the

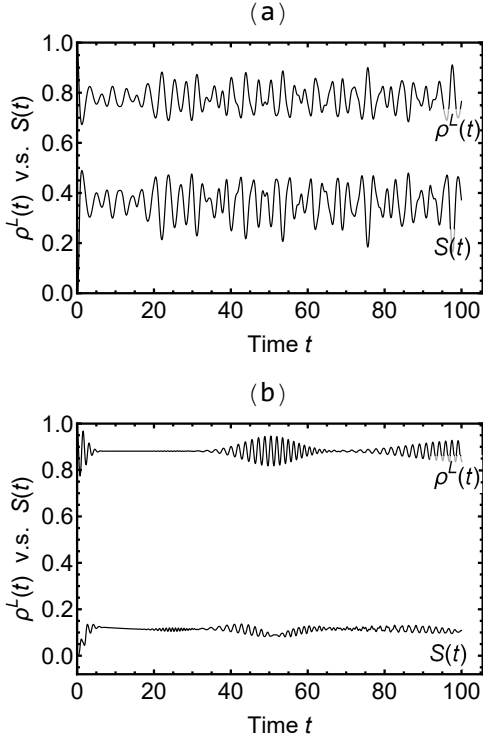


FIG. 5. Time-dependent linear entropy and population in $|L\rangle$ of an electron interacting with (a) a thermal state and (b) a coherent state of 16 photons in an isolated system. We observe an anti-correlation between the linear entropy and the population in (a), and collapses and revivals of Rabi oscillation with shortened time intervals in (b). The parameters are $\Delta_1 = \Delta = 0$ and $g = \Gamma = 1$.

population, shown in Fig. 5(b), with shortened intervals in time.³⁰ A possible explanation of the entropy-population anti-correlation is that the fluctuations in a thermal photon mode wash out much of the quantum interference effects between different levels. As a result, the purity of the electronic state is directly and solely determined by the overlap of the electron with the quasi-eigenstate $|L\rangle$, rather than by the complete quantum data stored in the wave function as a coherent superposition of $|L\rangle$, $|R\rangle$ and $|R^*\rangle$, as is the case when the electron interacts with a coherent photon mode.

B. Open system: suppressed relaxation kinetics

We now allow interaction of the three-level system with an environment via the excited level $|R^*\rangle$ and discuss the relaxation kinetics of an electron initially in $|L\rangle$ into the environment. We study this open system as a minimal model of the proposed traffic bottleneck in photosynthetic transport, instead of invoking a more formal treatment which requires the knowledge of microscopic details up and down the electron transport chain. We identify $|L\rangle$ with the immediate donors to P700⁺ and P680⁺, and neglect back-tunneling from $|L\rangle$ up the electron transport chain in the presence of a large redox gradient. A phenomenological parameter γ is used to characterize the irreversible relaxation rate from $|R^*\rangle$ to outside the

system when quantum correlations between $|L\rangle$, $|R\rangle$ and $|R^*\rangle$ are not considered. In general, various biochemical processes may contribute to γ . Here we focus on the transfer of photoexcited electrons by P700* and P680* to the immediate acceptors to form primary charge separations. Formally, γ may be calculated by the resolvent method if information about the interaction details with the environment is known.

For simplicity, we assume $\Delta_1 = \Delta = 0$ in the analytical treatment below, although the conclusion is not dependent of the convenient choice of parameters. We will first work with a Fock state of n photons interacting with the three-level system. Cases of a coherent state and a thermal state of photons are discussed later.

The Hamiltonian of the open system is $H' = H - (i\gamma/2)|R^*\rangle\langle R^*|$. We solve the eigenvalue problem by perturbation theory, assuming $\gamma/\lambda_n < 1$ to ensure convergence of the perturbative series. We define orthogonality of the eigenvectors of non-Hermitian operator H' using eigenvectors of its hermitian conjugate H'^\dagger ,³⁶ obtained by sending $\gamma \rightarrow -\gamma$ in H' .

The eigenvectors of H' are found to be

$$\begin{aligned} |0, n\rangle' &= |0, n\rangle - i\gamma \frac{\sin \theta_n \cos \theta_n}{2\sqrt{2}\lambda_n} (|+, n\rangle - |-, n\rangle), \\ |+, n\rangle' &= |+, n\rangle + i\gamma \left(\frac{\sin \theta_n \cos \theta_n}{2\sqrt{2}\lambda_n} |0, n\rangle - \frac{\cos^2 \theta_n}{8\lambda_n} |-, n\rangle \right), \\ |-, n\rangle' &= |-, n\rangle - i\gamma \left(\frac{\sin \theta_n \cos \theta_n}{2\sqrt{2}\lambda_n} |0, n\rangle - \frac{\cos^2 \theta_n}{8\lambda_n} |+, n\rangle \right), \end{aligned} \quad (24)$$

with eigenvalues $-i\kappa_0$, $\lambda_n - i\kappa$, $-\lambda_n - i\kappa$, respectively, where

$$\begin{aligned} \kappa_0 &= \frac{\gamma}{2} \sin^2 \theta_n, \\ \kappa &= \frac{\gamma}{4} \cos^2 \theta_n, \end{aligned} \quad (25)$$

and $|0, n\rangle$, $|+, n\rangle$ and $|-, n\rangle$ are the unperturbed eigenvectors in Eq. (4). We use these results to obtain time evolution of the system. Imagine in the distant past, the relaxation term was turned on adiabatically, and the eigenvectors gradually evolved into the ones in Eq. (24). At $t = 0$, an electron is fed in $|L\rangle$ with forbidden backward hopping. The total quantum state is described by Eq. (5) upon the replacements $|0, n\rangle \rightarrow |0, n\rangle'$, $|+, n\rangle \rightarrow |+, n\rangle'$ and $|-, n\rangle \rightarrow |-, n\rangle'$. The system then evolves according to the perturbed Hamiltonian H' . Because the perturbed eigenvectors do not coincide or collapse within the parameter range of interest (*i.e.*, no exceptional points exist), we can find time-dependent total wave function, as well as the diagonal elements of the reduced electron density matrix, using faithful eigenvector-decomposition of the initial wave function. In Fig. 6, we plot the probability that the electron remains in the initial state $|L\rangle$ at time t . It is clear that electron transport out of $|L\rangle$, and consequently from the system to the environment, is increasingly suppressed at larger photon numbers. This tendency is independent of the choice of γ , as long as the perturbation theory is well-defined, and persists in cases where $\Delta_1 \neq 0$ and $\Delta \neq 0$ (not shown).

To proceed, we average out the fast oscillations in $\rho^L(t)$,

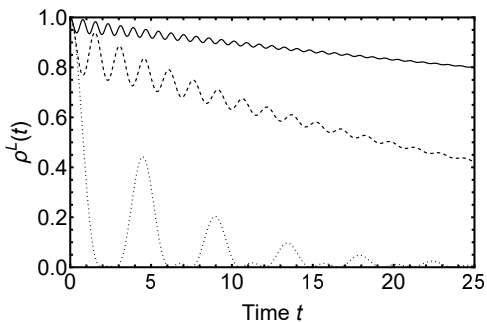


FIG. 6. Time-dependent population in $|L\rangle$ of an electron interacting with a Fock state of $n = 64$ (solid curve), $n = 16$ (dashed curve) and $n = 1$ (dotted curve) photons in an open system, where $\Delta_1 = \Delta = 0$, $g = \Gamma = 1$ and $\gamma = 0.5$.

$\rho^R(t)$, $\rho^{R^*}(t)$ as before and obtain

$$\begin{aligned} P_L(t) &= \cos^4 \theta_n e^{-2\kappa_0 t} + \frac{1}{2} \sin^4 \theta_n e^{-2\kappa t}, \\ P_R(t) &= \frac{1}{2} \sin^2 \theta_n e^{-2\kappa t}, \\ P_{R^*}(t) &= \sin^2 \theta_n \cos^2 \theta_n \left(e^{-2\kappa_0 t} + \frac{1}{2} e^{-2\kappa t} \right), \end{aligned} \quad (26)$$

respectively, where we have dropped the terms quadratic in γ/λ_n . We see that $P_L(t)$, $P_R(t)$ and $P_{R^*}(t)$ are all macroscopic quantities depending only on the relative light intensity ϵn and the product γt .

Using $\sin^2 \theta_n = 1/(1 + \epsilon n)$, we find $P_R(t), P_{R^*}(t) \ll 1$ for $\epsilon n \gg 1$. Thus, under steady, high light illumination, a significantly larger amount of charge accumulates in $|L\rangle$, compared to that under low light conditions. This underlies the physics of biphasic reduction kinetics of P700⁺ in PSI and the long-lived P680⁺ in PSII, as we discuss in Sec. III. Moreover, Eq. (26) tells that when the incident light is strong enough, the escape rate of an electron from the system is inversely proportional to the light intensity. To see this, notice that the probability that the electron leaves the system at time t is given by $1 - P_L(t) - P_R(t) - P_{R^*}(t)$, which for $\epsilon n \gg 1$ is well approximated by the leaked population $\delta P_L(t) = 1 - P_L(t)$ defined previously,

$$\delta P_L(t) \simeq 1 - \cos^4 \theta_n e^{-2\kappa_0 t}. \quad (27)$$

We identify $2\kappa_0 = \gamma/(1 + \epsilon n)$, the rate at which the electron is leaked out of $|L\rangle$, with the escape rate which in our interpretation is directly representative of the photochemical rate constant. Physically, this means that the photochemical efficiencies at PSI and PSII are governed by the reduction rates of P700⁺ and P680⁺.

We now argue that the above results obtained for a Fock state of photons apply also to a coherent state and a thermal state of photons. For a coherent state, the relative variation $\delta(\epsilon n)/\epsilon m_\alpha = \delta n/m_\alpha$ vanishes as $m_\alpha \rightarrow \infty$, using the statistical property of the Poisson distribution in Eq. (14). Thus, Eqs. (26)(27) with ϵn replaced by ϵm_α should be considered a good approximation in the macroscopic limit, in all light

conditions. For a thermal state, we notice that the exponential function in Eq. (27) may be expanded in high light conditions $\epsilon n \gg 1$, to obtain $\delta P_L(t) \simeq (2 + \gamma t)/(1 + \epsilon n)$ to leading order, where the only dependence on photon number is through the denominator. We can then perform a summation over photon number just as we did when studying an isolated three-level system (see Appendix B), to go from the results for a Fock state to those for a thermal state. From previous discussion, we know that the summation produces an additional logarithm factor $\ln \epsilon m_\beta$ reflecting weakening of the suppression effect.

In our simplified picture of photosynthetic transport, electrons are fed in $|L\rangle$ by LEF at a constant rate under steady illumination such that the local charge in the three-level system is nearly uniform in time. Then, the steady-state charge distribution may be approximated by Eq. (26) near $t = 0$, or simply Eq. (7) where the total population in the system is unity. Non-uniformity in the instantaneous local charge can be modeled by a deviation of the time parameter t from zero, and thus a less-than-unity total population, due to fluctuations in electron feeding times. For instance, a lower-than-average instantaneous charge is found when the previous electron has left the system but the next electron has not yet shown up as expected in $|L\rangle$. This non-uniformity is assumed to be small in steady state. An implication of this assumption is that when the intensity of incident light increases so that the escape rate of an electron is suppressed, the electron feeding rate, commensurate with the escape rate to ensure a conserved local charge, should also be lower. This is in fact discrepant with realistic data, and we will address this point when applying Eq. (26) to interpreting the light responses of PSI parameters.

In above discussion we have neglected relaxation of the electron within the system. In a fluorescence measurement of PSII, this corresponds to prompt signals originating from radiative decays of P680*. Such an event is incoherent and irreversible, and thus the electron will lose all the ‘‘memories’’ about previous trajectories. The electron then behaves no differently from an electron in the ground state of P680 at the beginning of time evolution, which can be excited independently and incoherently. At increasing intensities of incident light, collective quantum effects gradually establish dominance over incoherent excitation of electrons, which dynamically control the populations of P680 and P680⁺ in steady state, as we discuss in more detail in the next section.

III. DISCUSSION OF EXPERIMENTS

In the traditional view of photosynthetic charge transfer, forward hops of electrons are a series of independent, incoherent and irreversible events. Passing of a photoexcited electron to the immediate acceptor is fast enough that it does not constitute a bottleneck on LEF.¹⁶ The rate-limiting event is thus believed to be the PQ turnover between PSI and PSII.³⁷ When quantum correlations between charge donors and acceptors at photoexcitation are taken into account, however, this picture is challenged. As we have seen, when incident light is strong, the photochemical rate constant κ_P changes inversely propor-

tional to the intensity of light,

$$\kappa_P \propto \frac{\gamma}{1 + \varepsilon \langle n \rangle}, \quad (28)$$

where $\varepsilon \langle n \rangle$ is the relative light intensity. Quantum effects may suppress charge transfer from PC to P700 and from TyrZ to P680 so greatly that photoexcitation becomes the actual rate-limiting event. This blocking effect is a direct consequence of coherent driving by light and may be termed photo-blockade.

The limiting nature of charge transfer from PC was already revealed in early studies of transport in PSI. Under continuous illumination, it was found that partial inhibition of PC led to immediate decline of electron transport rate, contradicting the common belief that the much slower charge transfer from PQH₂ to Cyt *b6f* was the rate-limiting step.³² Inhibition of charge feeding from PSII did not change the results. In our picture, the moderate light used in the experiment was able to drive the system into the regime where Eq. (28) took control of the photosynthetic yield. Application of PC inhibitors reduced in time the statistical average of the transition amplitude Γ between PC and P700 (or equivalently raising ε), and consequently the photochemical rate constant κ_P .

Our model allows for a qualitative description of the light responses of the PSI parameters Y(I), Y(NA) and Y(ND),¹⁴ defined as the ratios of photo-redox active (oxidizable) P700, non-oxidizable P700 and P700⁺ to total P700, and commonly interpreted as the quantum yield of PSI, the acceptor-side limitation and the donor-side limitation on LEF, respectively. Applying the photo-blockade picture, however, Y(I), Y(NA) and Y(ND) are in fact correlated quantities that can be approximated, respectively, by the steady-state populations P_R^{ss} , P_R^{ss} and P_L^{ss} obtained by setting $t = 0$ in Eq. (26), plotted in Fig. 3. Physically, Y(NA) reflects a direct regulation by light of the steady-state population of P700* on the donor side,

$$Y(NA) \propto \frac{\varepsilon \langle n \rangle}{(1 + \varepsilon \langle n \rangle)^2}. \quad (29)$$

The advantage of this new interpretation is that it is consistent with the observation that shortage of PSI acceptors hardly occurs under steady-state conditions in the absence of extreme environmental stresses.³⁸ Eq. (29) reproduces the shape of the light response curve of Y(NA) to a reasonable accuracy.

The photo-blockade picture breaks down when the system is outside the regime of coherent photoexcitation, *e.g.*, in the dark or under extreme environmental stresses. In those cases, quantum correlations between charge donors and acceptors either have little influence on LEF or are destroyed, so that the restriction on Y(NA) is absent. For instance, in very dim light, when there is a large number of unoxidized P700 present, photoexcitation is largely incoherent, unregulated and independent of the charge transfer rate from PC to P700. Changing from extremely low light to moderately low light, charge gradually builds up in the PC pool, while photo-blockade becomes increasingly pronounced and then dominant. During this course, Y(I) experiences a rapid drop upon depletion of incoherently oxidizable P700 and eventually the population of oxidizable P700 is entirely determined by the reduction rate

of P700⁺. Likely signatures of such a transition in the nature of photoexcitation were recently reported.³⁹ Photo-blockade thus plays the role of a protective barrier against excess charge excitations. In extremely high light, or in the absence of ΔpH -inducing proteins such as PGR5 or PGRL1, a P700 reaction center may be temporarily or permanently inactivated due to insufficient dissipation of excess energy arriving from light-harvesting antennas and obstructed by photo-blockade. This causes overheating of PSI and destruction of quantum coherence, creating an over-reduced acceptor side with unregulated charge recombination,⁴ and a rapid rise in Y(NA) reflecting now the acceptor-side limitation.^{7,11,18}

When comparing Fig. 3 with typical data of PSI quantum yield,¹⁵ a marked deviation of Y(I) from P_R^{ss} and, to a lesser extent, a deviation of Y(ND) from P_L^{ss} are found. We explain these discrepancies by reconsidering the assumption of a conserved local charge that implies a light-suppressed charge flow through the local system, appearing to be inconsistent with the realistic situation. Indeed, under steady illumination the electron transport rate through PSI is known to grow with the intensity of irradiance before it saturates in very high light. This would mean a higher, rather than lower, electron feeding rate in higher light conditions and thus a larger steady-state local charge. One way to resolve this contradiction is to adopt a picture of “multi-channel” transport, each channel corresponding to an operating reaction center. While the steady-state populations and the transfer rate of an individual electron in one channel are given by Eq. (26) near $t = 0$ and Eq. (28), respectively, the number of operating channels increases linearly with the intensity of light. Viewed as the product of the transfer rate of electrons in one channel and the number of operating channels, the electron transport rate in fact describes the total transfer efficiency of all the channels subject to photo-blockade. An implication of this picture is the overestimation of Y(ND) by P_L^{ss} and the underestimation of Y(I) by P_R^{ss} , because when obtaining PSI quantum yield, it is the absolute populations of P700/P700⁺ that are measured, not the relative populations of the electrons associated with PC, (oxidizable) ground state P700, and (non-oxidizable) photoexcited P700*. At increasing light intensities, more free electrons are present in the local system at a given time, so that the actual population of P700⁺ being reduced is larger than that predicted by P_L^{ss} obtained in a single electron model assuming a complete measurement. This difference produces larger numerators of Y(I) and Y(NA), but a smaller numerator of Y(ND), while the denominators of the three quantities, the total number of P700 molecules, remain unchanged. Thus, Y(I) and Y(NA) should be greater than P_R^{ss} and P_R^{ss} , respectively, whereas Y(ND) is smaller than P_L^{ss} . Using $Y(I) + Y(NA) + Y(ND) = 1$, the total gain in Y(I) and Y(NA) due to the contribution of additional free electrons may be thought of as from the loss in Y(ND). A further insight in these changes comes from the ratio

$$\frac{P_R^{ss}}{P_R} \propto \frac{\varepsilon \langle n \rangle}{1 + \varepsilon \langle n \rangle}, \quad (30)$$

which shows that in low light electrons tend to dwell in $|R\rangle$ rather than in $|R^*\rangle$, and consequently a significant portion of the loss in Y(ND) goes to Y(I) rather than to Y(NA), corre-

sponding to a substantial increase in the population of oxidizable P700. This explains the rise in the light response curve of Y(I) immediately from zero light, in contrast to a decline in that of P_R^{ss} . It also explains the much deeper dip in the light response curve of Y(ND) than that of P_L^{ss} . This dip can touch zero in low light, which implies that all the $P700^+$ have been reduced by LEF, before being re-oxidized by photo-blockade in higher light. On the other hand, when $\varepsilon\langle n \rangle \gg 1$, Y(I) and Y(NA) share the loss in Y(ND) evenly as the electron transport rate saturates. The second-order deviations of Fig. 3 from realistic data may be attributed to feedback processes not addressed in our minimal model.

Reduction kinetics of $P700^+$ after saturating light illumination was found to exhibit biphasic features, suggesting an inhomogeneous redox equilibration down the electron transport chain. This was proposed to result from the slow lateral diffusion of PC restricted by the space in the thylakoid lumen.^{19,20} Upon turning off illumination, a rapid local charge transfer between bound state PC and $P700^+$ occurs first on a time scale of tens of microseconds, before LEF from Cyt *b6f* reduces the rest of oxidized molecules to achieve global redox balance. Photo-blockade does not challenge this interpretation, but provides a mechanism explaining the local charge imbalance between PC and P700 when illumination is on. Due to finite diffusion times of PC, steady-state charge distribution of the local system described by Eq. (26) cannot be established immediately, despite the dynamic nature of photo-blockade. Thus, when measured with a short flash,²¹ reduction kinetics of $P700^+$ reflects the one-shot nature of incoherent photoexcitation $P700 \rightarrow P700^*$, which is monophasic and independent of the supply of electrons from PC.

Eq. (28) is applicable to explaining the light response data of PSII parameters in moderate to high light, where the charge transfer efficiency at PSII is determined by photo-blockade. To this end, however, one is reminded that the equation is based on a donor-side scheme, whereas current interpretation of fluorescence measurements is based on the conceived limitation on the acceptor side,^{16,17} where a reduced quinone acceptor is thought to produce a “closed” reaction center. While it is tempting to connect κ_p with the fraction of “open” centers in a “puddle” model or a “lake” model, whose light responses indeed bear some resemblance,⁴⁰ it should be clear that these are quantities of distinct origins. In particular, κ_p should be understood as a holistic parameter characterizing the operating efficiency of PSII, *e.g.*, corresponding to in the acceptor-side scheme the combined limiting effects of the degree of openness of reaction centers and the maximum yield of an open reaction center. In the donor-side scheme, the notion of openness/closedness of a reaction center controlled by the redox state of the quinone acceptor loses significance. Moreover, the phenomenological parameter γ may depend on various environmental conditions such as temperature and carbon dioxide concentration. The same applies to the transition amplitude Γ , which is expected to grow with temperature,³¹ leading to a diminished ε . Together γ and ε decide the shape of the light response curve of PSII quantum yield, while the light response of NPQ follows a compensatory pattern. We note that a nonzero detuning Δ also affects the shape of a light response

curve, in which case the photo-blockade picture is still valid, as was shown in Sec. II and evidenced experimentally.⁴¹ The functioning of photo-blockade relies on the presence of continuous illumination. For instance, when measured with short light pulses, charge transfer from TyrZ to P680 occurs on a time scale of tens to hundreds of nanoseconds and is not rate-limiting in photosynthetic transport.³⁷

The donor-side picture of photo-blockade was motivated also by data from photodamaged PSII. Once considered of acceptor-side origins,²² photodamage is now believed to take place at the oxygen-evolving complex.^{23–28} It was revealed that the rate constant of this first-order damaging reaction was directly proportional to the intensity of incident light, opposing the assumption that it was caused by unregulated excess excitations in the chloroplast. A recently proposed two-step mechanism hypothesizes that excitation of manganese ions by light inactivates the oxygen-evolving complex and blocks charge transfer from TyrZ to P680.^{25,26} Aggregation of highly oxidizing $P680^+$ then leads to irreversible damage to reaction centers. This theory is supported by the evidence that the initial rate of photodamage is unaffected by the inhibition of acceptor-side electron transport and ATP synthesis, as well as various environmental stresses.²⁴ An interpretation by photo-blockade agrees with the manganese mechanism that photodamage results from inappropriate oxidation of functional components in PSII by long-lived $P680^+$. However, instead of postulating an impaired oxygen-evolving complex in the beginning stage, we suggest that the suppressed charge transfer from normally functioning oxygen-evolving complex to P680 by direct and dynamic action of light is responsible for the lowered reduction rate of $P680^+$. This picture enjoys the advantage of simplicity, explains the high sensitivity of photodamage to low light, and does not depend on the absorption and transfer of energy between light-harvesting antennas or from antennas to reaction centers.

IV. CONCLUDING REMARKS

We proposed a new dynamic mechanism to explain the modulation of photochemical efficiencies under varying light conditions, taking into consideration quantum correlations between donor and acceptor molecules in electron transport. The declines in the quantum yields of PSI and PSII at increasing irradiance were attributed to light-driven blockade of charge transfer from PC to P700 and from TyrZ to P680, respectively. Using a minimal model of three quantum levels, we derived a set of formulas that describe the light response curves of PSI and PSII parameters. The model also offers a consistent interpretation of a series of experiments, including PC-dependent electron transport, biphasic reduction kinetics of $P700^+$, and wavelength dependent quantum yields, as well as recent data from photodamaged PSII. These demonstrate that quantum coherence plays an important role in not only the excitonic energy transfer but the charge transfer processes.

As a direct test of our proposal, we suggest a measurement of the quantum yield of PSII with different light sources. Quantum mechanically, light emanating from a laser and from

a filtered incandescent lamp may be approximated, respectively, by a coherent and a thermal state of photons. An observable difference is expected in the tails of the light response curves measured with a lamp and with a laser. In the former case, thermal fluctuation weakens the blockade effect by light and thus one may find a higher quantum yield at a given light intensity. The difference should be more pronounced in high light conditions, where the dependences on light intensity of leaked population δP_L and of escape rate $2\kappa_0$ coincide (see the discussion below Eq. (27)) and the logarithm factor in Eq. (21) may manifest itself directly in the data. In addition, one may observe an apparent growth of the quantum yield with temperature in the case of lamp illumination, because mean photon number in a thermal state is positively correlated with temperature. In principle, the same measurement may be conducted on PSI. However, PSI is more vulnerable than PSII to photo-damage in high light, and the data may be obscured by feedback processes. We expect the measurement on PSII to be more revealing of the effect of thermal fluctuation.

The mechanism proposed in this work is a very general effect that may find evidence beyond photosynthetic organisms. Microscopically, suppression of electron tunneling over a prolonged period of time produces abnormally high concentrations of certain reactants in biochemical processes which may slow down the reactions and induce irreversible mutations, *e.g.*, in DNA molecules. In a larger scope and on a much longer time scale, regional and temporal patterns of accumulation of solar-radiation-related mutations may constitute a dynamic factor behind non-gradual morphological changes of species,^{42,43} serving as an example of macroscopic irreversibility from microscopic reversibility.

ACKNOWLEDGEMENT

We thank Dr. Anton Kockum for valuable comments. This work was supported by JSPS KAKENHI Grant Number 21H01034.

Appendix A: Analytic solution for degenerate $|L\rangle$ and $|R\rangle$

In this appendix, we solve the time-dependent Schrödinger equation analytically, assuming $|L\rangle$ and $|R\rangle$ are degenerate, $\Delta_1 = 0$. Substituting the wave function in Eq. (3) of the main text, the Schrödinger equation becomes

$$\begin{pmatrix} \dot{c}_{1,n} \\ \dot{c}_{2,n} \\ \dot{c}_{3,n} \end{pmatrix} = -iH_n \begin{pmatrix} c_{1,n} \\ c_{2,n} \\ c_{3,n} \end{pmatrix}. \quad (\text{A1})$$

The solution takes the form

$$\begin{pmatrix} c_{1,n}(t) \\ c_{2,n}(t) \\ c_{3,n}(t) \end{pmatrix} = a(t) \begin{pmatrix} c_{1,n}(0) \\ c_{2,n}(0) \\ c_{3,n}(0) \end{pmatrix}, \quad (\text{A2})$$

with $c_{1,n}(0) = 1$, $c_{2,n}(0) = 0$, and $c_{3,n}(0) = 0$ given that the electron is initially in $|L\rangle$. Using orthogonality of the eigenvectors of H_n , one can show that $a(t)$ is a symmetric matrix.

We solve Eq. (A1) by Laplace transform and the theory of cubic equations. The elements of $a(t)$ are found to be,

$$\begin{aligned} a_{11} &= \frac{\lambda_1^2 - \Delta\lambda_1 - g_n^2}{(\lambda_1 - \lambda_2)(\lambda_1 - \lambda_3)} e^{-i\lambda_1 t} + \frac{\lambda_2^2 - \Delta\lambda_2 - g_n^2}{(\lambda_2 - \lambda_1)(\lambda_2 - \lambda_3)} e^{-i\lambda_2 t} + \frac{\lambda_3^2 - \Delta\lambda_3 - g_n^2}{(\lambda_3 - \lambda_1)(\lambda_3 - \lambda_2)} e^{-i\lambda_3 t}, \\ a_{12} &= \frac{(\lambda_1 - \Delta)\Gamma}{(\lambda_1 - \lambda_2)(\lambda_1 - \lambda_3)} e^{-i\lambda_1 t} + \frac{(\lambda_2 - \Delta)\Gamma}{(\lambda_2 - \lambda_1)(\lambda_2 - \lambda_3)} e^{-i\lambda_2 t} + \frac{(\lambda_3 - \Delta)\Gamma}{(\lambda_3 - \lambda_1)(\lambda_3 - \lambda_2)} e^{-i\lambda_3 t}, \\ a_{13} &= \frac{g_n\Gamma}{(\lambda_1 - \lambda_2)(\lambda_1 - \lambda_3)} e^{-i\lambda_1 t} + \frac{g_n\Gamma}{(\lambda_2 - \lambda_1)(\lambda_2 - \lambda_3)} e^{-i\lambda_2 t} + \frac{g_n\Gamma}{(\lambda_3 - \lambda_1)(\lambda_3 - \lambda_2)} e^{-i\lambda_3 t}, \\ a_{22} &= \frac{(\lambda_1 - \Delta)\lambda_1}{(\lambda_1 - \lambda_2)(\lambda_1 - \lambda_3)} e^{-i\lambda_1 t} + \frac{(\lambda_2 - \Delta)\lambda_2}{(\lambda_2 - \lambda_1)(\lambda_2 - \lambda_3)} e^{-i\lambda_2 t} + \frac{(\lambda_3 - \Delta)\lambda_3}{(\lambda_3 - \lambda_1)(\lambda_3 - \lambda_2)} e^{-i\lambda_3 t}, \\ a_{23} &= \frac{g_n\lambda_1}{(\lambda_1 - \lambda_2)(\lambda_1 - \lambda_3)} e^{-i\lambda_1 t} + \frac{g_n\lambda_2}{(\lambda_2 - \lambda_1)(\lambda_2 - \lambda_3)} e^{-i\lambda_2 t} + \frac{g_n\lambda_3}{(\lambda_3 - \lambda_1)(\lambda_3 - \lambda_2)} e^{-i\lambda_3 t}, \\ a_{33} &= \frac{\lambda_1^2 - \Gamma^2}{(\lambda_1 - \lambda_2)(\lambda_1 - \lambda_3)} e^{-i\lambda_1 t} + \frac{\lambda_2^2 - \Gamma^2}{(\lambda_2 - \lambda_1)(\lambda_2 - \lambda_3)} e^{-i\lambda_2 t} + \frac{\lambda_3^2 - \Gamma^2}{(\lambda_3 - \lambda_1)(\lambda_3 - \lambda_2)} e^{-i\lambda_3 t}, \end{aligned} \quad (\text{A3})$$

where the real numbers

$$\begin{aligned} \lambda_1 &= \frac{\Delta}{3} - 2\sqrt{-P} \cos\left(\frac{1}{3} \arccos \frac{Q}{2(-P)^{\frac{3}{2}}}\right), \\ \lambda_2 &= \frac{\Delta}{3} - 2\sqrt{-P} \cos\left(\frac{1}{3} \arccos \frac{Q}{2(-P)^{\frac{3}{2}}} + \frac{2\pi}{3}\right), \\ \lambda_3 &= \frac{\Delta}{3} - 2\sqrt{-P} \cos\left(\frac{1}{3} \arccos \frac{Q}{2(-P)^{\frac{3}{2}}} - \frac{2\pi}{3}\right) \end{aligned} \quad (\text{A4})$$

are eigenvalues of H_n , with

$$\begin{aligned} P &= -\frac{\Delta^2}{9} - \frac{\Gamma^2 + g_n^2}{3}, \\ Q &= -\frac{2\Delta^3}{27} - \frac{(g_n^2 - 2\Gamma^2)\Delta}{3}. \end{aligned} \quad (\text{A5})$$

At zero detuning $\Delta = 0$, the expressions of the eigenvalues are

greatly simplified,

$$\begin{aligned}\lambda_1 &= -\lambda_n, \\ \lambda_2 &= \lambda_n, \\ \lambda_3 &= 0,\end{aligned}\quad (\text{A6})$$

where $\lambda_n = \sqrt{\Gamma^2 + g_n^2}$.

Appendix B: Leaked population for a coherent state and a thermal state of photons

In this appendix, we obtain compact expressions of leaked population δP_L in an isolated system. For a coherent state of photons, we start with Eq. (16) in the main text. The summation in $\delta P_{L;1}$ was encountered in the study of linear response of a charged Bose gas immerse in an external magnetic field, and was known to produce a confluent hypergeometric function. The summation in $\delta P_{L;2}$ produces a generalized hypergeometric function. We find

$$\begin{aligned}\delta P_{L;1} &= 2e^{-m_\alpha} {}_1F_1\left(\frac{1}{\varepsilon}; 1 + \frac{1}{\varepsilon}; m_\alpha\right), \\ \delta P_{L;2} &= \frac{3}{2}e^{-m_\alpha} {}_2F_2\left(\frac{1}{\varepsilon}, \frac{1}{\varepsilon}; 1 + \frac{1}{\varepsilon}, 1 + \frac{1}{\varepsilon}; m_\alpha\right),\end{aligned}\quad (\text{B1})$$

where ${}_1F_1(a; b; x)$ and ${}_2F_2(a_1, a_2; b_1, b_2; x)$ are Kummer's confluent hypergeometric function and the generalized hypergeometric function, respectively. When the mean photon number $m_\alpha \gg 1$, the contribution from $\delta P_{L;2}$ is negligible, and we focus on examining $\delta P_{L;1}$. The expression of $\delta P_{L;1}$ is greatly simplified for symmetric bare parameters $\Gamma = g$,

$$\delta P_{L;1}|_{\varepsilon=1} = \frac{2}{m_\alpha}(1 - e^{-m_\alpha}), \quad (\text{B2})$$

showing a similar behavior to $\delta P_{L;1}|_{\varepsilon=1}$ for a Fock state of photons at large photon numbers.

For a general ε , we invoke the previously obtained asymptotic expansion of Kummer's function,⁴⁴

$$\begin{aligned}\delta P_{L;1} &= \frac{2}{1 + \varepsilon m_\alpha} \left(1 + \frac{m_\alpha}{(m_\alpha + \varepsilon^{-1})^2} - \frac{m_\alpha}{(m_\alpha + \varepsilon^{-1})^3} \right. \\ &\quad \left. + \frac{3m_\alpha^2 + m_\alpha}{(m_\alpha + \varepsilon^{-1})^4} + \dots \right),\end{aligned}\quad (\text{B3})$$

valid for $m_\alpha \gg 1$ and $\varepsilon \ll 1$. Keeping the first two terms in the bracket we obtain Eq. (17) in the main text.

For a thermal state of photons, we start with Eq. (20) in the main text. The summations yield

$$\begin{aligned}\delta P_{L;1} &= \frac{2}{m_\beta + 1} {}_2F_1\left(1, \frac{1}{\varepsilon}; 1 + \frac{1}{\varepsilon}; \frac{m_\beta}{m_\beta + 1}\right), \\ \delta P_{L;2} &= \frac{3/2}{m_\beta + 1} {}_3F_2\left(1, \frac{1}{\varepsilon}, \frac{1}{\varepsilon}; 1 + \frac{1}{\varepsilon}, 1 + \frac{1}{\varepsilon}; \frac{m_\beta}{m_\beta + 1}\right),\end{aligned}\quad (\text{B4})$$

where ${}_2F_1(a_1, a_2; b; x)$ is the Gauss hypergeometric function and ${}_3F_2(a_1, a_2, a_3; b_1, b_2; x)$ is a generalized hypergeometric

function. Eq. (B4) is easily verified using the series definitions of the hypergeometric functions. At large photon numbers, $\delta P_{L;2}$ is negligible as in the case of a coherent state of photons. For symmetric bare parameters, we have

$$\begin{aligned}\delta P_{L;1}|_{\varepsilon=1} &= \frac{2}{m_\beta} \ln(m_\beta + 1), \\ \delta P_{L;2}|_{\varepsilon=1} &= \frac{3/2}{m_\beta} \text{Li}_2\left(\frac{m_\beta}{m_\beta + 1}\right),\end{aligned}\quad (\text{B5})$$

where $\text{Li}_2(x)$ is the polylogarithm function of order 2. Eq. (B5) manifests the logarithm factor in δP_L , a characteristic feature of a thermal state.

To proceed, we obtain the asymptotic expansion

$$\begin{aligned}\delta P_{L;1} &= \frac{2}{\varepsilon(m_\beta + 1)} \sum_{n=0}^{\infty} \frac{\prod_{k=0}^n (1 + k\varepsilon)}{1 + n\varepsilon} \\ &\quad \times \frac{\ln(m_\beta + 1) - \psi(n + \varepsilon^{-1}) + \psi(n + 1)}{n! \varepsilon^n (m_\beta + 1)^n}\end{aligned}\quad (\text{B6})$$

valid for $m_\beta \gg 1$, where $\psi(x)$ is the digamma function. To see that Eq. (B6) produces a sensible macroscopic limit, consider the lowest-order terms in the summation. Naively, $\ln(m_\beta + 1)$ and $\psi(\varepsilon^{-1})$ are singular when $m_\beta \rightarrow \infty$ and $\varepsilon \rightarrow 0$. However, using the asymptotic expression of the digamma function with a large argument $x \gg 1$,⁴⁵

$$\psi(x + s) = \ln x + \sum_{n=1}^{\infty} \frac{(-)^{n+1} B_n(s)}{n} x^{-n}, \quad (\text{B7})$$

where s can be a real number and $B_n(s)$ are Bernoulli polynomials, we find

$$\ln(m_\beta + 1) - \psi(\varepsilon^{-1}) \simeq \ln \varepsilon (m_\beta + 1) + \frac{\varepsilon}{2}. \quad (\text{B8})$$

One can check using Eq. (B7) that the higher-order terms are also regular in the macroscopic limit.

When $\varepsilon \gg 1$, one can use the series definition of the digamma function,⁴⁵

$$\psi(x) = -\gamma_0 - \frac{1}{x} + \sum_{n=1}^{\infty} \frac{x}{n(x+n)}, \quad (\text{B9})$$

where γ_0 is Euler's constant, to show that Eq. (B6) is still regular. However, in such a strong-coupling limit, *e.g.*, when the electron-photon coupling strength g is of a comparable order of magnitude with that of the photon energy ω , it is known that the rotating-wave approximation in the Jaynes-Cummings model breaks down and the model becomes unphysical. In particular, the ground state of the system will no longer be one involving the vacuum state of photons.⁴⁶

Finally, when $\varepsilon = 1$, the summation reduces to a geometric series which recovers the expression in Eq. (B5). We conclude that Eq. (B6) is well-defined in a large domain of ε .

We emphasize here that $\delta P_{L;1}$ is a good approximation of δP_L only at large photon numbers in a finite-size system, or at high light intensities in free space. Otherwise, one must resort

to the exact results in Eqs. (B1)(B4) for an accurate estimation of δP_L . Keeping the lowest-order terms in the summation in Eq. (B6), using Eq. (B8), and sending $\varepsilon \rightarrow 0$ for the macroscopic limit, we obtain Eq. (21) in the main text.

- ¹M. Kono and I. Terashima, *J. Photoch. Photobio. B* **137**, 89 (2014).
- ²K. Takizawa, J. A. Cruz, A. Kanazawa, and D. M. Kramer, *Biochim. Biophys. Acta* **1767**, 1233 (2007).
- ³P. Müller, X.-P. Li, and K. K. Niyogi, *Plant Physiol.* **125**, 1558 (2001).
- ⁴Y. Munekage, M. Hojo, J. Meurer, T. Endo, M. Tasaka, and T. Shikanai, *Cell* **110**, 361 (2002).
- ⁵G. DalCorso, P. Pesaresi, S. Masiero, E. Aseeva, D. Schönemann, G. Finazzi, P. Joliot, R. Barbato, and D. Leister, *Cell* **132**, 273 (2008).
- ⁶C. Wang, H. Yamamoto, and T. Shikanai, *Biochim. Biophys. Acta* **1847**, 931 (2015).
- ⁷M. Kono, K. Noguchi, and I. Terashima, *Plant Cell Physiol.* **55**, 990 (2014).
- ⁸P. Joliot and A. Joliot, *Biochim. Biophys. Acta* **1757**, 362 (2006).
- ⁹M. Tikkanen, S. Rantala, and E.M. Aro, *Front. Plant Sci.* **6**, 521 (2015).
- ¹⁰G. Shimakawa and C. Miyake, *Plant Direct* **2**, e00073 (2018).
- ¹¹M. Zivcak, M. Brestic, K. Kunderlikova, O. Sytar, and S. I. Allakhverdiev, *Photosynth. Res.* **126**, 449 (2015).
- ¹²W. Huang, Y.-J. Yang, S.-B. Zhang, and T. Liu, *Front. Plant Sci.* **9**, 239 (2018).
- ¹³T. Mirkovic, E. E. Ostroumov, J. M. Anna, R. van Grondelle, Govindjee, and G. D. Scholes, *Chem. Rev.* **117**, 249 (2017).
- ¹⁴C. Klughammer and U. Schreiber, *Planta* **192**, 261 (1994).
- ¹⁵C. Klughammer and U. Schreiber, *PAM Application Notes* **1**, 11 (2008).
- ¹⁶G. Krause and E. Weis, *Annu. Rev. Plant Physiol. Plant Mol. Biol.* **42**, 313 (1991).
- ¹⁷N. R. Baker, *Annu. Rev. Plant Biol.* **59**, 89 (2008).
- ¹⁸W. Huang, S.-B. Zhang, and K.-F. Cao, *Plant Cell Physiol.* **51**, 1922 (2010).
- ¹⁹F. Drepper, M. Hippler, W. Nitschke, and W. Haehnel, *Biochemistry* **35**, 1282 (1996).
- ²⁰H. Kirchhoff, C. Hall, M. Wood, M. Herbstová, O. Tsabari, R. Nevo, D. Charuvi, E. Shimoni, and Z. Reich, *Proc. Natl. Acad. Sci. U.S.A.* **108**, 20248 (2011).
- ²¹G. Finazzi, F. Sommer, and M. Hippler, *Proc. Natl. Acad. Sci. U.S.A.* **102**, 7031 (2005).
- ²²I. Vass, S. Styring, T. Hundal, A. Koivuniemi, E.M. Aro, and B. Andersson, *Proc. Natl. Acad. Sci. U.S.A.* **89**, 1408 (1992).
- ²³E. Tyystjärvi and E.M. Aro, *Proc. Natl. Acad. Sci. U.S.A.* **93**, 2213 (1996).
- ²⁴S. I. Allakhverdiev, Y. Nishiyama, S. Takahashi, S. Miyairi, I. Suzuki, and N. Murata, *Plant Physiol.* **137**, 263 (2005).
- ²⁵M. Hakala, I. Tuominen, M. Keränen, T. Tyystjärvi, and E. Tyystjärvi, *Biochim. Biophys. Acta* **1706**, 68 (2005).
- ²⁶N. Ohnishi, S. I. Allakhverdiev, S. Takahashi, S. Higashi, M. Watanabe, Y. Nishiyama, and N. Murata, *Biochemistry* **44**, 8494 (2005).
- ²⁷C. Jegerschöld, I. Virgin, and S. Styring, *Biochemistry* **29**, 6179 (1990).
- ²⁸H. J. Eckert, B. Geiken, J. Bernarding, A. Napiwotzki, H. J. Eichler, and G. Renger, *Photosyn. Res.* **27**, 97 (1991).
- ²⁹M. Grieco, M. Suorsa, A. Jajoo, M. Tikkanen, and E.M. Aro, *Biochim. Biophys. Acta* **1847**, 607 (2015).
- ³⁰B. W. Shore and P. L. Knight, *J. Mod. Optics* **40**, 1195 (1993).
- ³¹R. A. Marcus and N. Sutin, *Biochim. Biophys. Acta* **811**, 265 (1985).
- ³²W. Haehnel, *Biochim. Biophys. Acta* **682**, 245 (1982).
- ³³R. F. Werner, *Phys. Rev. A* **40**, 4277 (1989).
- ³⁴C. Cohen-Tannoudji, J. Dupont-Roc, and G. Grynberg, *Atom-Photon Interactions: Basic Processes and Applications*, Wiley-VCH (2004).
- ³⁵R. Pariser, *J. Chem. Phys.* **24**, 250 (1956).
- ³⁶M. M. Sternheim and J. F. Walker, *Phys. Rev. C* **6**, 114 (1972).
- ³⁷W. Haehnel, *Annu. Rev. Plant Physiol.* **35**, 659 (1984).
- ³⁸N. R. Baker, J. Harbinson, and D. M. Kramer, *Plant Cell Environ.* **30**, 1107 (2007).
- ³⁹C. Miyake, *Antioxidants* **9**, 230 (2020).
- ⁴⁰D. M. Kramer, G. Johnson, O. Kiirats, and G. E. Edwards, *Photosynth. Res.* **79**, 209 (2004).
- ⁴¹S. W. Hogewoning, E. Wientjes, P. Douwstra, G. Trouwborst, W. Van Ieperen, R. Croce, and J. Harbinson, *Plant Cell* **24**, 1921 (2012).
- ⁴²G. B. Müller and S. A. Newman, eds., *Origination of Organismal Form: Beyond the Gene in Developmental and Evolutionary Biology*, The MIT Press, Cambridge (2003).
- ⁴³S. J. Gould and N. Eldredge, *Paleobiology* **3**, 115 (1977).
- ⁴⁴V. Kowalenko and N. E. Frankel, *J. Math. Phys.* **35**, 6179 (1994).
- ⁴⁵Y. L. Luke, *The Special Functions and their Approximations*, Vol. I, Academic Press, New York (2002).
- ⁴⁶H. Azuma and M. Ban, *Int. J. Mod. Phys. C* **22**, 1015 (2011).